Development of bio-composites with novel characteristics: Evaluation of phenol-induced antibacterial, biocompatible and biodegradable behaviours

Dr Hafiz Iqbal[1]
Dr Godfrey Kyazze[1]
Dr Ian Locke[1]
Thierry Tron[2]
Prof Taj Keshavarz[1]

[1] Faculty of Science and Technology, University of Westminster, London, UK
[2] Aix Marseille Université, CNRS, Marseille, France

"NOTICE: this is the author's version of a work that was accepted for publication in *Carbohydrate Polymers*. Changes resulting from the publishing process, such as peer review, editing, corrections, structural formatting, and other quality control mechanisms may not be reflected in this document. Changes may have been made to this work since it was submitted for publication. A definitive version was subsequently published in Carbohydrate Polymers, 131 (2015), 197-207, doi: 10.1016/j.carbpol.2015.05.046"

Development of bio-composites with novel characteristics: Evaluation of phenol-induced antibacterial, biocompatible and biodegradable behaviours

Hafiz M. N. Iqbal[a,*], Godfrey Kyazze[a], Ian C. Locke[a], Thierry Tron[b], Tajalli Keshavarz [a,*]

[a] Applied Biotechnology Research Group, Department of Life Sciences, Faculty of Science and Technology, University of Westminster London, W1W 6UW, United Kingdom; [b] Aix-Marseille Université, CNRS, Centrale Marseille, iSm2 UMR 7313, 13397 Marseille, France. *Corresponding author Tel.: +44 020 79115030; fax: +44 020 79115087; E-mail addresses: hafiz.iqbal@my.westminster.ac.uk (H.M.N. Iqbal), t.keshavarz@westminster.ac.uk (T. Keshavarz).

Abstract

This paper describes a laccase-assisted grafting of gallic acid (GA) and thymol (T) as functional entities onto the previously developed P(3HB)-*g*-EC composite. GA-*g*-P(3HB)-*g*-EC and T-*g*-P(3HB)-*g*-EC bio-composites were prepared by laccase-assisted free radical-induced graft polymerisation of GA and T onto the P(3HB)-*g*-EC based composite using surface dipping and incorporation technique. The results of the antibacterial evaluation for the prepared composites indicated that 15GA-*g*-P(3HB)-*g*-EC, 15T-*g*-P(3HB)-*g*-EC and 20T-*g*-P(3HB)-*g*-EC composites possessed the strongest bacteriostatic and bactericidal activities against Gram-positive *B. subtilis* NCTC 3610 and *S. aureus* NCTC 6571 and Gram-negative *E. coli* NTCT 10418 and *P. aeruginosa* NCTC 10662 strains. In this study, we have also tested GA-*g*-P(3HB)-*g*-EC and T-*g*-P(3HB)-*g*-EC bio-composites for their ability to support and maintain multilineage differentiation of human keratinocyte-like (HaCaT) skin cells *in-vitro*. From the cytotoxicity results, the tested composites showed 100% viability and did not

induce any adverse effect on a HaCaT's morphology. Finally, in soil burial evaluation, a progressive increase in the degradation rate of GA-*g*-P(3HB)-*g*-EC and T-*g*-P(3HB)-*g*-EC bio-composites was recorded with the passage of time up to 6 weeks. In summary, our current findings suggest that GA-*g*-P(3HB)-*g*-EC and T-*g*-P(3HB)-*g*-EC bio-composites are promising candidates for biomedical type applications such as skin regeneration, multiphasic tissue engineering and/or medical implants.

Keywords: Laccase; Bio-composite, Gallic acid; Thymol; Antibacterial; HaCaT compatible

1. Introduction

In recent years, with the increasing emergence of infectious diseases caused by various microorganisms, there is an urgent need for the development of non-toxic green polymeric materials and/or composites with antimicrobial activity. Laccase-assisted grafting has recently been the focus of green chemistry technologies in response to the growing environmental concerns, legal restrictions and advances in science. In principle, laccase-assisted grafting may modify and/or impart a variety of new functionalities to the materials of interest as the modified materials through grafting have boundless applications (Božič et al., 2012; Iqbal et al., 2014a).

In recent years, with increasing consciousness to reduce, and preferably eradicate a bacterial population in healthcare facilities and possibly to cut pathogenic infections, development of materials with novel characteristics are considered with urgency. The antibacterial features of silver nanoparticles have been reported, however, excess release of silver nanoparticles inhibits osteoblasts growth and consequently can also cause many severe side effects such as cytotoxicity (Sandukas et al., 201; Albers et al., 2013; Wang et al., 2014). In this context,

there is a need for green composites with antimicrobial activity to reduce or even eliminate the risk of bacterial infection without cytotoxicity.

Antimicrobial products may be fabricated by introducing antimicrobial agents through surface coating or dipping, spraying or incorporating microbicidal functional groups with cellulose (Dong et al., 2014). However, in practice, the main drawback of the various physical/chemical methods is the risk of premature delamination and short-term antibacterial effects (Hiriart-Ramı´rez et al., 2012). On the other hand, laccase-assisted grafting and incorporation of microbicidal groups, such as natural phenols seems to be a promising technique. This technique offers clean and safe alternative to the currently practiced physical/chemical methods (Chen et al., 2000; Aljawish et al., 2012). In the production of functional materials, enzyme specificity may offer the potential to better control the polymer function through precise modifications in the polymer structure (Chen et al., 2000; Yamada et al., 2000; Iqbal et al., 2014b,c).

It is well-known that phenols are typical laccase substrates because their redox potentials are low enough to allow electron abstraction by Cu1 reaction site of the laccase. They are oxidized into phenoxy radicals which, depending on the reaction conditions, can spontaneously polymerize via radical coupling, or rearrange themselves into highly-reactive quinones through a disproportionate mechanism. Figure 1 illustrates a schematic mechanism for laccase action in the preparation of phenol grafted P(3HB)-*g*-EC composites. Among the tested phenolic structures GA and T, both have pronounced antibacterial features toward a wide spectrum of Gram-positive and Gram-negative bacteria. In addition, their flavouring, antioxidant and antiseptic characteristics has already been reported elsewhere by several authors (Sanchez-Garcia et al. 2008; Archana et al. 2011; Rukmani and Sundrarajan 2012; Shahidi et al., 2014). On the basis of these evidences, we hypothesised that GA and T may be efficient candidates for inhibiting bacterial infections. Thus we developed a series of novel

bio-composites *e.g.*, GA-*g*-P(3HB)-*g*-EC and T-*g*-P(3HB)-*g*-EC and investigated their biocompatibility and antibacterial activity *in-vitro* against human keratinocytes-like cell, and Gram-positive and Gram-negative bacterial strains respectively.

2. Materials and Methods

2.1. Chemicals

Dulbecco's modified eagle's medium (DMEM), phosphate buffer saline (PBS), streptomycin and was penicillin were obtained from Lonza, UK. Fetal calf serum was received from Labtech International Ltd., UK. Table 1 illustrates physiochemical characteristics of GA and T obtained from Sigma-Aldrich Company Ltd., UK.

2.2. Microorganisms

B. subtilis NCTC 3610, *S. aureus* NCTC 6571, *E. coli* NTCT 10418 and *P. aeruginosa* NCTC 10662 strains were obtained from the culture collection unit of the University of Westminster London, UK. An overnight grown inoculum of each of the aforementioned strains was developed, separately, in 50 mL sterile nutrient broth under temperature controlled environment at 30 °C and 120 rpm.

2.3. Grafting of phenols onto P(3HB)-*g*-EC

The grafting of GA and T onto the previously developed P(3HB)-*g*-EC composite (Iqbal et al., 2014b), was performed via surface dipping and incorporation technique. A pre-weight P(3HB)-*g*-EC was dipped in a 50 mL solution of GA and T, separately. Control sample, [P(3HB)-*g*-EC], was treated with buffer alone without GA and/or T. After the stipulated reaction time (60 min), the weight of each composite was recorded followed by incubation at

50 ^{o}C until fully dried and final dry weight was recorded. The dried films were designated as GA-*g*-P(3HB)-*g*-EC bio-composites *i.e.,* [0GA-*g*-P(3HB)-*g*-EC (control); 5GA-*g*-P(3HB)-*g*-EC; 10GA-*g*-P(3HB)-*g*-EC; 15GA-*g*-P(3HB)-*g*-EC and 20GA-*g*-P(3HB)-*g*-EC] and T-*g*-P(3HB)-*g*-EC bio-composites *i.e.,* [0T-*g*-P(3HB)-*g*-EC (control); 5T-*g*-P(3HB)-*g*-EC; 10T-*g*-P(3HB)-*g*-EC; 15T-*g*-P(3HB)-*g*-EC and 20T-*g*-P(3HB)-*g*-EC] and used as prepared for further evaluation.

2.4. Fourier Transform Infrared spectroscopy (FT-IR)

The individual and grafted composites were placed on the diamond crystal, and infrared absorption spectra were recorded from the wavelength region of 4000-500 cm^{-1} using a Perkin Elmer System 2000 FT-IR spectrophotometer. All spectra were collected with 64 scans and 2 cm^{-1} resolution and assigned peak numbers.

2.5. Grafting parameters

The grafting parameters *i.e.,* graft yield (GY %), grafting efficiency (GE %) and swelling ratio (SR %) behaviours of the GA-*g*-P(3HB)-*g*-EC and T-*g*-P(3HB)-*g*-EC bio-composites were investigated. The aforementioned parameters were calculated according to the following equations with minor modifications as reported earlier by Sabaa et al., 2012.

$$\text{Graft yield (GY\%)} = [(Wf - Wi) / Wi] \times 100 \quad (1)$$

$$\text{Grafting efficiency (GE\%)} = [(Wf - Wi) / (Ws - Wi)] \times 100 \quad (2)$$

$$\text{Swelling ratio (SR\%)} = Ws - Wi / Wi \times 100 \quad (3)$$

Where, Wi = initial weight before immersion; Wf = final dry weight after immersion; and Ws = weight of sample at the swollen state

2.6. Antibacterial activity assay

The antibacterial activities of GA-*g*-P(3HB)-*g*-EC and T-*g*-P(3HB)-*g*-EC bio-composites were inspected against Gram-positive (*B. subtilis* NCTC 3610 and *S. aureus* NCTC 6571) and Gram-negative (*E. coli* NTCT 10418 and *P. aeruginosa* NCTC 10662) strains. An overnight grown spore suspensions of each bacteria were inoculated on the pre-sterilised surfaces of GA-*g*-P(3HB)-*g*-EC and T-*g*-P(3HB)-*g*-EC bio-composites, followed by incubation in a temperature controlled incubator at 30 °C for 24 h. After the stipulated incubation time period (24 h), the bacterial cells were washed twice using 50 mL phosphate buffer (pH, 7.0) and the viable cells were calculated as CFU/mL by conventional spread-plate method by serial dilution. In comparison to control (initial bacterial count *i.e.,* 10^5 CFU/mL), the mean colony forming units per mL (CFU/mL) values were used to calculate the reduction in log value by using the Equation 4.

$$\text{Log reduction} = \log \text{CFU control sample} - \log \text{CFU treated sample} \quad (4)$$

2.7. *In-vitro* cell viability assay

To evaluate the cytotoxicity of the newly synthesised GA-*g*-P(3HB)-*g*-EC and T-*g*-P(3HB)-*g*-EC bio-composites a human keratinocytes-like HaCaT cell line was adopted, in this study. HaCaT cell viability was measured after 1, 3 and 5 days of incubation using neutral red assay as reported earlier (Iqbal et al., 2015). The HaCaT cell viability in percentage was calculated using the Equation 5. Whereas, the adherent morphology of HaCaT cells seeded on the P(3HB)-*g*-EC, GA-*g*-P(3HB)-*g*-EC and T-*g*-P(3HB)-*g*-EC bio-composites was observed using Nikon light microscope. After 1 h incubation in neutral red dye solution, the stained cells were washed with PBS prior to record images at 100× magnification.

$$\% \text{ cell viability} = \frac{OD_{\text{Test specimen}} - OD_{\text{Negative control}}}{OD_{\text{Positive control}}} \times 100 \quad (5)$$

Standard tissue culture plastic was used as a positive control whereas graft composite without cell culture was used as negative control to normalise the absorption of the neutral red dye by the graft composite itself.

2.8. Soil Burial Test

The biodegradability of GA-*g*-P(3HB)-*g*-EC and T-*g*-P(3HB)-*g*-EC bio-composites was evaluated using soil burial test as-described earlier by Wattanakornsiri et al., 2012. After every 7 days of burial, each set was removed, washed, dried and subsequently weighed to determine the loss in weight, being recorded every week for 6 weeks. The percentage of weight loss was calculated using the Equation 6.

$$\% \text{ Loss in weight} = \frac{\text{Control weight} - \text{loss in weight}}{\text{Control weight}} \times 100 \quad (6)$$

3. Results and Discussion

The FT-IR spectra were used to characterise the structural elements of GA, T, P(3HB)-*g*-EC, GA-*g*-P(3HB)-*g*-EC and T-*g*-P(3HB)-*g*-EC (shown in Figure 2A and B). For GA-*g*-P(3HB)-*g*-EC, the absorptions at 3345, 1720, 1360, and 1056 cm^{-1} in the spectrum are indications of GA. The region between 1260 and 1056 cm^{-1} relates to the C–H and C–O–C bond stretching frequencies; a band at 2985 cm^{-1} is assigned to C–H vibration; the band range from 3200 to 3400 cm^{-1} corresponds to the vibration stretching of inter- and intramolecular hydrogen bonds of GA-*g*-P(3HB)-*g*-EC. The peak at 1000–1150 cm^{-1}, corresponding mainly to ethers (C–O–C), increased compared to phenolics monomers spectra, indicating extended polymerisation (Yamada et al., 2007). It has typical polyphenol characteristics, showing broad peaks centred at 3345 and 1375 cm^{-1} due to the vibration of O–H linkage of phenolic and hydroxyl groups, at 1450–1600 cm^{-1} due to the aromatic ring C=C stretching, and C=O stretching vibration at 1200–1300 cm^{-1}, respectively. A new peak at 1625 cm^{-1} is probably due to the quinone

moiety absorption. The most intense peaks at 738 and 807 cm^{-1} are assigned to ring vibrations of the T chemistry (Schulz et al., 2003; Torres-Giner et al., 2014). Figure 2B depict an increase in the hydrogen bond peak at 3360 cm^{-1} as a result of T affinity to the P(3HB)-*g*-EC, this peak was not found in the spectra of pristine T. The T-*g*-P(3HB)-*g*-EC spectra exhibit a different profile compared to the spectra of pure T alone. The bands in the 3070–2860 cm^{-1} region are assigned to the C–H, CH_2 and CH_3 vibrations. In the fingerprint region, there are bands assigned to the aromatic and hetero aliphatic rings as well as to the CH_2 and CH_3 modes. The peak at 1000–1150 cm^{-1}, corresponding mainly to C-O-C linkages, increased compared to phenolics monomers spectra, indicating extended polymerisation (Yamada et al., 2007; Božič et al., 2012). By comparison between this and the T-*g*-P(3HB)-*g*-EC spectra, it can be seen that some bands changed intensity and/or shape during the graft formation process.

Figs. 3 A and B shows the graft yield (GY%), grafting efficiency (GE%) and swelling ratio (SR%) profiles of GA-*g*-P(3HB)-*g*-EC *i.e.*, 0GA-*g*-P(3HB)-*g*-EC, 5GA-*g*-P(3HB)-*g*-EC, 10GA-*g*-P(3HB)-*g*-EC, 15GA-*g*-P(3HB)-*g*-EC and 20GA-*g*-P(3HB)-*g*-EC and T-*g*-P(3HB)-*g*-EC *i.e.,* 0T-*g*-P(3HB)-*g*-EC, 5T-*g*-P(3HB)-*g*-EC, 10T-*g*-P(3HB)-*g*-EC, 15T-*g*-P(3HB)-*g*-EC and 20T-*g*-P(3HB)-*g*-EC bio-composites. A consistent increase in all of the grafting parameters *i.e.,* GY%, GE% and SR% was recorded up to the concentration of 15 mM GA, whereas, in case of T 20 mM concentration was proved best under the same environment. However, further increase up to 20 mM GA concentration showed decreasing trend in aforementioned parameters. One possible reason for the observed behaviour could be the substantial amount of GA grafted onto the P(3HB)-*g*-EC bio-composite, which creates steric hindrance for further grafting. The increase in monomer concentration would be expected to increase both the grafting percentage which in turn increase the molecular weight of the graft

composite (Aggour, 2001; Constantin et al., 2011). Indeed, the results presented in Figure 3 indicate that as the concentration of GA increases from 0 to 15 mM both the GY% and GE% were optimal with an increase in the swelling ratio. The order of GP % observed for GA-*g*-P(3HB)-*g*-EC and T-*g*-P(3HB)-*g*-EC composites was: 15GA-*g*-P(3HB)-*g*-EC > 10GA-*g*-P(3HB)-*g*-EC > 20GA-*g*-P(3HB)-*g*-EC > 5GA-*g*-P(3HB)-*g*-EC > 0GA-*g*-P(3HB)-*g*-EC and 20T-*g*-P(3HB)-*g*-EC >15T-*g*-P(3HB)-*g*-EC > 10T-*g*-P(3HB)-*g*-EC > 5T-*g*-P(3HB)-*g*-EC > 0T-*g*-P(3HB)-*g*-EC respectively. It has also been reported in literature that the reaction time is an important parameter which can increase or decrease the grafting parameters like graft yield, grafting efficiency and swelling behaviour (Sun et al., 2003; Constantin et al., 2011).

The results of the disc diffusion method for GA-*g*-P(3HB)-*g*-EC bio-composites against each bacterial strain are given in the Fig. 4 (A-D). 0GA-*g*-P(3HB)-*g*-EC used as a control, did not showed any log reduction (CFU/mL) against *B. subtilis* NCTC 3610, *S. aureus* NCTC 6571, *E. coli* NTCT 10418 and *P. aeruginosa* NCTC 10662, thus showing no antibacterial potentials. 5GA-*g*-P(3HB)-*g*-EC and 20GA-*g*-P(3HB)-*g*-EC composites prepared with 5 and 20 mM GA concentration, respectively, did not show any potential to inhibit bacterial count against each of the above said bacterial species. However, the composite prepared by the incorporation of 10 and 15 mM GA onto P(3HB)-*g*-EC backbone material displayed excellent antibacterial activities against all of the tested species (Fig. 4, A-D). For the samples prepared in the presence of laccase, the results clearly show that increasing the concentration of T the antibacterial activity is enhanced, reaching a complete bactericidal effect at 20 mM concentration against test microorganisms. As already seen in Fig. 5 (A-D), the bio-composites, prepared with varying T concentrations (0 to 20 mM) in the presence of laccase, produced a slight bacteriostatic effect on *B. subtilis* NCTC 3610 and *S. aureus* NCTC 6571, in the range 15 and 20 mM concentration. The same composites with the same

concentration showed complete bactericidal effect on *E. coli* NTCT 10418 and *P. aeruginosa* NCTC 10662. The counting test showed a complete bactericidal effect (100 % reduction of bacterial count) on *E. coli* NTCT 10418 and *S. aureus* NCTC 6571, but only in the case of graft composites prepared with 15 mM and 20 mM T concentrations. This is because the interaction between T and bacteria can change the metabolic activity of bacteria and eventually cause their death. However, the exact mechanism of the antimicrobial action of T is not established yet. Based on an earlier publication, T has an ability to disrupt the lipid structure of the bacterial cell wall leading to the destruction of the cell membrane, cytoplasmic leakage, and cell lysis and ultimately, cell death (Veras et al. 2012; Milovanovic et al., 2013; Shahidi et al., 2014).

Cell viability at 1, 3 and 5 days after seeding of HaCaT cells on the GA-*g*-P(3HB)-*g*-EC and T-*g*-P(3HB)-*g*-EC bio-composites, in comparison to those on the tissue culture plastic (polystyrene), are shown in Fig. 6 (A-F). The GA and T grafted bio-composites supported variable viability of HaCaT cells. The % viability of HaCaT cells at 5 days of incubation on GA and T grafted bio-composites were in the following order: 10GA-*g*-P(3HB)-*g*-EC > 15GA-*g*-P(3HB)-*g*-EC > 5GA-*g*-P(3HB)-*g*-EC > 20GA-*g*-P(3HB)-*g*-EC > 0GA-*g*-P(3HB)-*g*-EC, and 15T-*g*-P(3HB)-*g*-EC > 20T-*g*-P(3HB)-*g*-EC > 10T-*g*-P(3HB)-*g*-EC > 5T-*g*-P(3HB)-*g*-EC > 0T-*g*-P(3HB)-*g*-EC. The Morphology of HaCaT cells grown on the GA-*g*-P(3HB)-*g*-EC and T-*g*-P(3HB)-*g*-EC bio-composites at 1, 3 and 5 days of seeding is shown in Figs. 7 and 8, respectively. HaCaT cells responded to the test composites by exhibiting good attachment and spreading. Moreover, the growing HaCaT cells demonstrated normal cell morphology with their typical shape and spread covering the material surface.

Figs. 9 and 10 shows the degradation profiles of the GA-*g*-P(3HB)-*g*-EC composites and T-*g*-P(3HB)-*g*-EC composites after 6 weeks of soil burial degradation, respectively. Owing to the difficulty in isolating degraded part of the test samples from soil particles, the weight loss of composites induced by biodegradation in soil was recorded. Figs. 9 and 10 illustrate the % weight loss of the test composites as a function of degradation time. All of the composites showed an increased degradation rate to different extents during the burial period. In contrast to the results obtained with the soil burial test, a significant difference was revealed in this experiment with respect to degradation rate. It was observed that the degradation rate of the pristine P(3HB)-*g*-EC was lower than that of the GA and/or T incorporated GA-*g*-P(3HB)-*g*-EC and T-*g*-P(3HB)-*g*-EC bio-composites. After 6 weeks of incubation, up to 100% bio-degradability of GA-*g*-P(3HB)-*g*-EC and T-*g*-P(3HB)-*g*-EC bio-composites was recorded in comparison to the control sample. Mostly, the cellulosic based composites/blends can be degraded by a wide spectrum of cellulolytic or ligninolytic enzymes secreted by the soil bacteria or fungi. For example brown rot fungi are more effective in decomposing cellulose and hemicelluloses like components, whereas, white rot fungi are able to degrade phenol containing structures like lignin. Moreover, such natural process factually simulates the degradation situation when the used composites are abandoned as garbage.

4. Conclusions

In conclusion, we prepared a series of novel bio-composites with natural phenols as functional entities which displayed an excellent antibacterial activity against Gram-positive and Gram-negative bacterial strains. The improved bacterial resistance along with human keratinocytes-like HaCaT compatibility indicate that the newly synthesised GA-*g*-P(3HB)-*g*-EC and T-*g*-P(3HB)-*g*-EC bio-composites are promising candidates for biomedical type applications such as skin regeneration, multiphasic tissue engineering and/or medical

implants. However further studies, especially *in-vivo* experiments are required for detailed information for other applications such as biomedical implants of these newly developed bio-composites.

Acknowledgements

This work was supported by the Cavendish Research Scholarship program of the University of Westminster London UK, a specialised research fund for the Doctoral Program for the University of Westminster Scholars.

References

Aggour, Y. A. (2001). Reaction kinetics of graft copolymerization and thermochemical studies of the degradation of poly(vinyl alcohol) graft copolymer. *Polymer International*, *50*, 347-353.

Albers, C. E., Hofstetter, W., Siebenrock, K. A., Landmann, R., & Klenke, F. M. (2013). In vitro cytotoxicity of silver nanoparticles on osteoblasts and osteoclasts at antibacterial concentrations. *Nanotoxicology*, *7*(1), 30-36.

Aljawish, A., Chevalot, I., Piffaut, B., Rondeau-Mouro, C., Girardin, M., Jasniewski, J., & Muniglia, L. (2012). Functionalization of chitosan by laccase-catalyzed oxidation of ferulic acid and ethyl ferulate under heterogeneous reaction conditions. *Carbohydrate Polymers*, *87*(1), 537-544.

Archana, P. R., Rao, B. N., & Rao, B. S. (2011). Modulation of gamma ray–induced genotoxic effect by thymol, a monoterpene phenol derivative of cymene. *Integrative Cancer Therapies*, *10*(4), 374-383.

299 Božič, M., Gorgieva, S., & Kokol, V. (2012). Homogeneous and heterogeneous methods for
300 laccase-mediated functionalization of chitosan by tannic acid and
301 quercetin. *Carbohydrate Polymers, 89(3)*, 854-864.
302 Chen, T., Kumar, G., Harris, M. T., Smith, P. J., & Payne, G. F. (2000). Enzymatic grafting
303 of hexyloxyphenol onto chitosan to alter surface and rheological properties.
304 *Biotechnology and Bioengineering, 70*(5), 564-573.
305 Constantin, M., Mihalcea, I., Oanea, I., Harabagiu, V., & Fundueanu, G. (2011). Studies on
306 graft copolymerization of 3-acrylamidopropyl trimethyl ammonium chloride on
307 pullulan. *Carbohydrate Polymers, 84(3)*, 926-932.
308 Dong, C., Ye, Y., Qian, L., Zhao, G., He, B., & Xiao, H. (2014). Antibacterial modification
309 of cellulose fibers by grafting β-cyclodextrin and inclusion with ciprofloxacin.
310 *Cellulose, 21(3)*, 1921-1932.
311 Hiriart-Ramı´rez, E., Contreras-Garcı´a, A., Garcia-Fernandez, M. J., Concheiro, A., Alvarez-
312 Lorenzo, C., Bucio, E. (2012). Radiation grafting of glycidyl methacrylate onto cotton
313 gauzes for functionalization with cyclodextrins and elution of antimicrobial agents.
314 *Cellulose, 19(6)*, 2165-2177.
315 Iqbal, H. M. N., Kyazze, G., Locke, I. C., Tron, T., & Keshavarz, T. (2015). *In-situ*
316 development of self-defensive antibacterial biomaterials: phenol-*g*-keratin-EC based
317 bio-composites with characteristics for biomedical applications. *Green Chemistry*, In-
318 Press, DOI: 10.1039/C5GC00715A.
319 Iqbal, H. M. N., Kyazze, G., Tron, T., & Keshavarz, T. (2014a). Laccase-assisted grafting of
320 poly (3-hydroxybutyrate) onto the bacterial cellulose as backbone polymer:
321 Development and characterisation. *Carbohydrate polymers, 113*, 131-137.

Iqbal, H. M. N., Kyazze, G., Tron, T., & Keshavarz, T. (2014b). A preliminary study on the development and characterisation of enzymatically grafted P (3HB)-ethyl cellulose based novel composites. *Cellulose, 21*(5), 3613-3621.

Iqbal, H. M. N., Kyazze, G., Tron, T., & Keshavarz, T. (2014c). "One-pot" synthesis and characterisation of novel P (3HB)–ethyl cellulose based graft composites through lipase catalysed esterification. *Polymer Chemistry, 5(24),* 7004-7012.

Milovanovic, S., Stamenic, M., Markovic, D., Radetic, M., & Zizovic, I. (2013). Solubility of thymol in supercritical carbon dioxide and its impregnation on cotton gauze. *The Journal of Supercritical Fluids, 84*, 173-181.

Rukmani, A., & Sundrarajan, M. (2012). Inclusion of antibacterial agent thymol on β-cyclodextrin-grafted organic cotton. *Journal of Industrial Textiles, 42*(2), 132-144.

Sabaa, M. W., Mohamed, N. A., Mohamed, R. R., Khalil, N. M., & Abd El Latif, S. M. (2010). Synthesis, characterization and antimicrobial activity of poly (N-vinyl imidazole) grafted carboxymethyl chitosan. *Carbohydrate Polymers, 79*(4), 998-1005.

Sanchez-Garcia, M. D., Ocio, M. J., Gimenez, E., & Lagaron, J. M. (2008). Novel polycaprolactone nanocomposites containing thymol of interest in antimicrobial film and coating applications. *Journal of Plastic Film and Sheeting, 24*(3-4), 239-251.

Sandukas, S., Yamamoto, A., & Rabiei, A. (2011). Osteoblast adhesion to functionally graded hydroxyapatite coatings doped with silver. *Journal of Biomedical Materials Research Part A, 97*(4), 490-497.

Schulz, H., Quilitzsch, R., & Krüger, H. (2003). Rapid evaluation and quantitative analysis of thyme, origano and chamomile essential oils by ATR-IR and NIR spectroscopy. *Journal of Molecular Structure, 661*, 299-306.

Shahidi, S., Aslan, N., Ghoranneviss, M., & Korachi, M. (2014). Effect of thymol on the antibacterial efficiency of plasma-treated cotton fabric. *Cellulose, 21*(3), 1933-1943.

Sun, T., Xu, P., Liu, Q., Xue, J., & Xie,W. (2003). Graft copolymerization ofmethacrylic acid onto carboxymethyl chitosan. *European Polymer Journal, 39,* 189-192.

Torres-Giner, S., Martinez-Abad, A., & Lagaron, J. M. (2014). Zein-based ultrathin fibers containing ceramic nanofillers obtained by electrospinning. II. Mechanical properties, gas barrier, and sustained release capacity of biocide thymol in multilayer polylactide films. *Journal of Applied Polymer Science. 131*, 40768.

Veras, H. N., Rodrigues, F. F., Colares, A. V., Menezes, I. R., Coutinho, H. D., Botelho, M. A., & Costa, J. G. (2012). Synergistic antibiotic activity of volatile compounds from the essential oil of Lippia sidoides and thymol. *Fitoterapia, 83*(3), 508-512.

Wang, L., He, S., Wu, X., Liang, S., Mu, Z., Wei, J., Deng, F., deng, Y., & Wei, S. (2014). Polyetheretherketone/nano-fluorohydroxyapatite composite with antimicrobial activity and osseointegration properties. *Biomaterials, 35*, 6758-6775.

Wattanakornsiri, A., Pachana, K., Kaewpirom, S., Traina, M., & Migliaresi, C. (2012). Preparation and properties of green composites based on tapioca starch and differently recycled paper cellulose fibers. *Journal of Polymers and the Environment*, *20*(3), 801-809.

Yamada, K., Abe, T., & Tanizawa, Y. (2007). Black tea stain formed on the surface of teacups and pots. Part 2—Study of the structure change caused by aging and calcium addition. *Food Chemistry, 103*, 8-14.

Yamada, K., Chen, T., Kumar, G., Vesnovsky, O., Topoleski, L. T., & Payne, G. F. (2000). Chitosan based water-resistant adhesive. Analogy to mussel glue. *Biomacromolecules, 1*(2), 252-258.

Figure captions

Figure 1 A tentative schematic representation of a proposed mechanism of graft formation through laccase-assisted grafting of gallic acid (as a model phenolic structure) onto the P(3HB)-*g*-EC based material. There are other possibilities too to depict the proposed mechanism of graft formation between phenol (used) and P(3HB)-*g*-EC based material.

Figure 2 FT-IR spectra; **(A)** gallic acid (GA) and GA-*g*-P(3HB)-*g*-EC bio-composites and **(B)** thymol (T) and T-*g*-P(3HB)-*g*-EC bio-composites.

Figure 3 Evaluation of grafting parameters *i.e.*, graft yield (GY %), grafting efficiency (GE %) and swelling ratio (SR %) behaviours of GA-*g*-P(3HB)-*g*-EC bio-composites **(A)** and T-*g*-P(3HB)-*g*-EC bio-composites **(B).**

Figure 4 Antimicrobial activity of GA-*g*-P(3HB)-*g*-EC composites against *B. subtilis* NCTC 3610 **(A)**; *S. aureus NCTC* 6571 **(B)**; *E. coli NTCT* 10418 **(C)** and *P. aeruginosa NCTC* 10662 **(D)**.

Figure 5 Antimicrobial activity of T-*g*-P(3HB)-*g*-EC bio-composites against *B. subtilis* NCTC 3610 **(A)**; *S. aureus NCTC* 6571 **(B)**; *E. coli NTCT* 10418 **(C)** and *P. aeruginosa NCTC* 10662 **(D)**.

Figure 6 Neutral red dye concentration dependent percentage cell viability of HaCaT cells seeded on the GA-*g*-P(3HB)-*g*-EC bio-composites **(A)** 1 day; **(B)** 3 days and **(C)** 5 days; and HaCaT cells seeded on the T-*g*-P(3HB)-*g*-EC bio-composites **(D)** 1 day; **(E)** 3 days; **(F)** 5 days.

Figure 7 Adherent morphology of HaCaT cells seeded on the GA-*g*-P(3HB)-*g*-EC bio-composites. All of the test samples were stained using neutral red dye (5 mg/mL) for 1 h followed by three consecutive washings with PBS at an ambient temperature.

Figure 8 Adherent morphology of HaCaT cells seeded on the T-*g*-P(3HB)-*g*-EC bio-composites. All of the test samples were stained using neutral red dye (5 mg/mL) for 1 h followed by three consecutive washings with PBS at an ambient temperature.

Figure 9 Effect of soil burial period on the biodegradability of GA-*g*-P(3HB)-*g*-EC bio-composites *i.e.,* 0GA-*g*-P(3HB)-*g*-EC (⬚), 5GA-*g*-P(3HB)-*g*-EC (▤), 10GA-*g*-P(3HB)-*g*-EC (▩), 15GA-*g*-P(3HB)-*g*-EC (▧) and 20GA-*g*-P(3HB)-*g*-EC (■) buried for prescribed periods *i.e.,* **(A)** 7 days; **(B)** 14 days; **(C)** 21 days; **(D)** 28 days; **(E)** 35 days and **(F)** 42 days.

Figure 10 Effect of soil burial period on the biodegradability of T-*g*-P(3HB)-*g*-EC bio-composites *i.e.,* 0T-*g*-P(3HB)-*g*-EC (⬚), 5T-*g*-P(3HB)-*g*-EC (▤), 10T-*g*-P(3HB)-*g*-EC (▩), 15T-*g*-P(3HB)-*g*-EC (▧) and 20T-*g*-P(3HB)-*g*-EC (■) buried for prescribed periods *i.e.,* **(A)** 7 days; **(B)** 14 days; **(C)** 21 days; **(D)** 28 days; **(E)** 35 days and **(F)** 42 days.

List of Figures

Figure 1

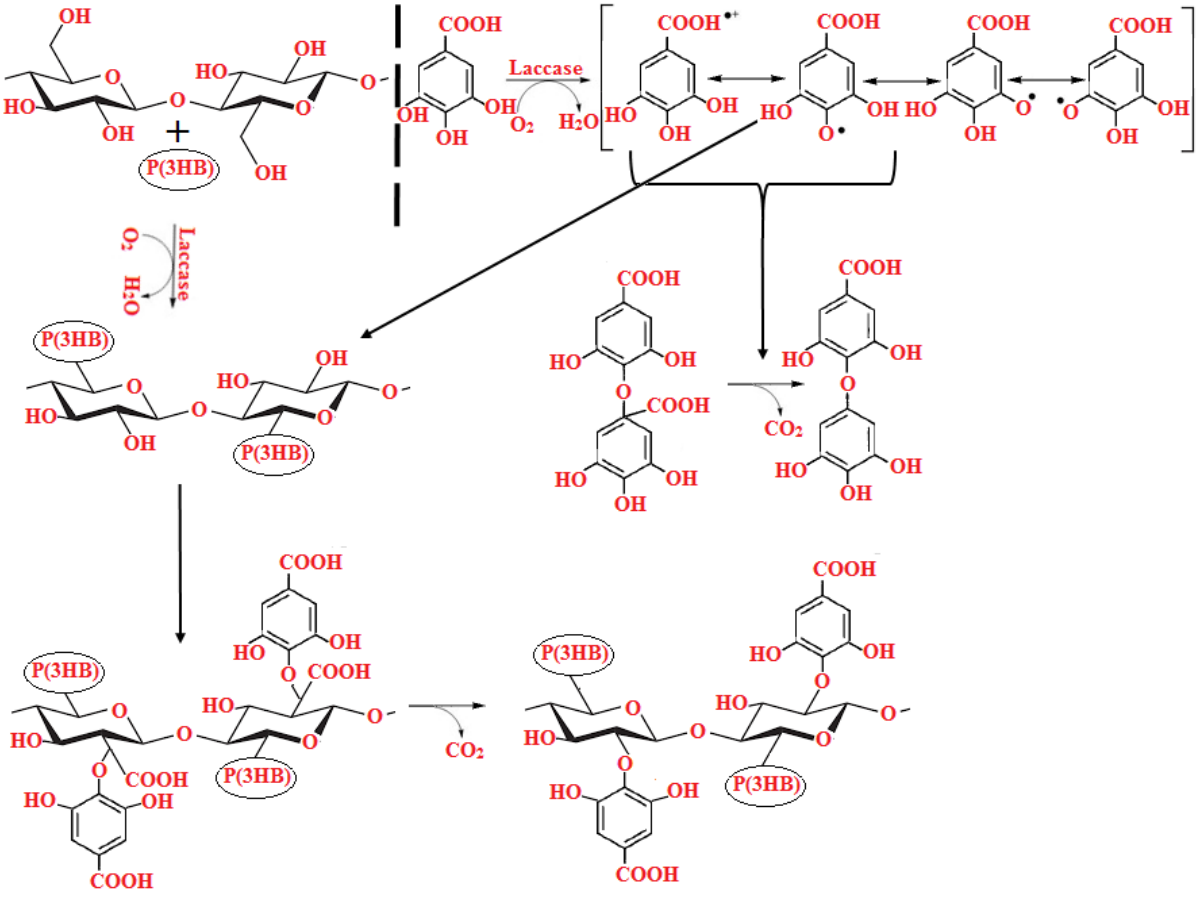

Figure 2 A

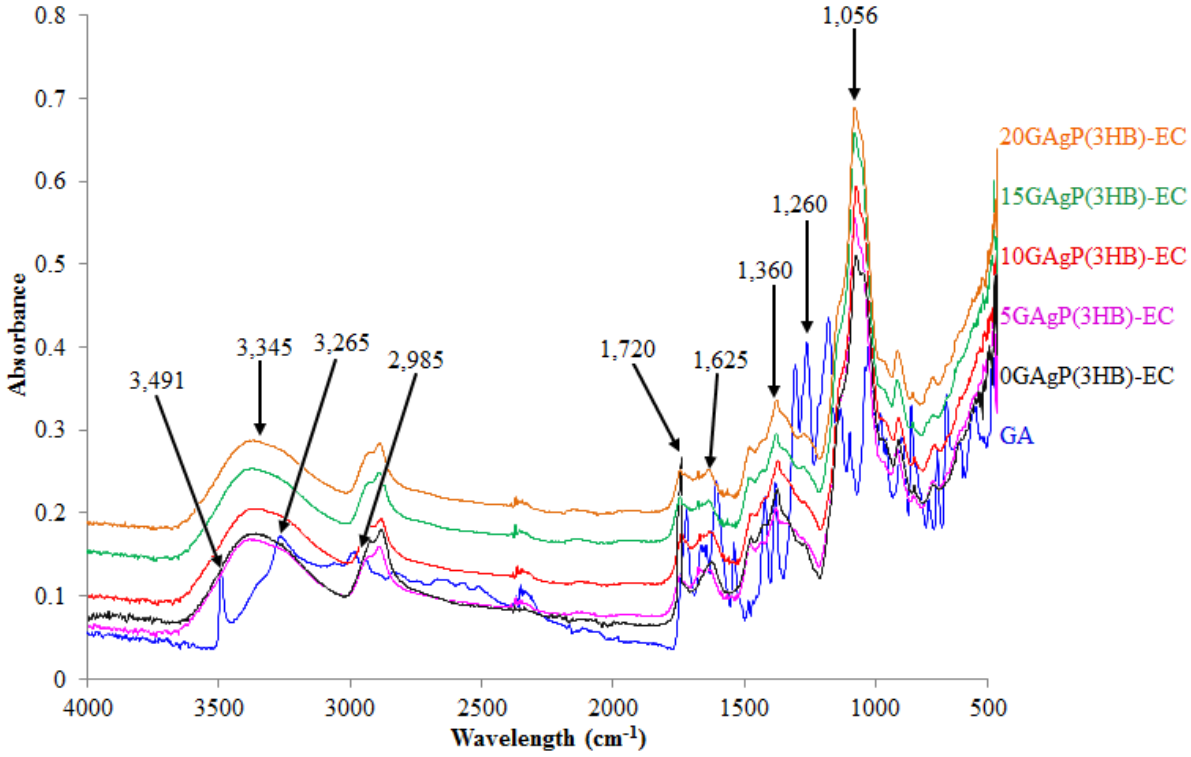
0.8
0.7
0.6
0.5
0.4
0.3
0.2
0.1
0
Absorbance
4000
3500
3000
2500
2000
1500
1000
500
Wavelength (cm-1)
3,491
3,345
3,265
2,985
1,720
1,625
1,360
1,260
1,056
20GAgP(3HB)-EC
15GAgP(3HB)-EC
10GAgP(3HB)-EC
5GAgP(3HB)-EC
0GAgP(3HB)-EC
GA

Figure 2 B

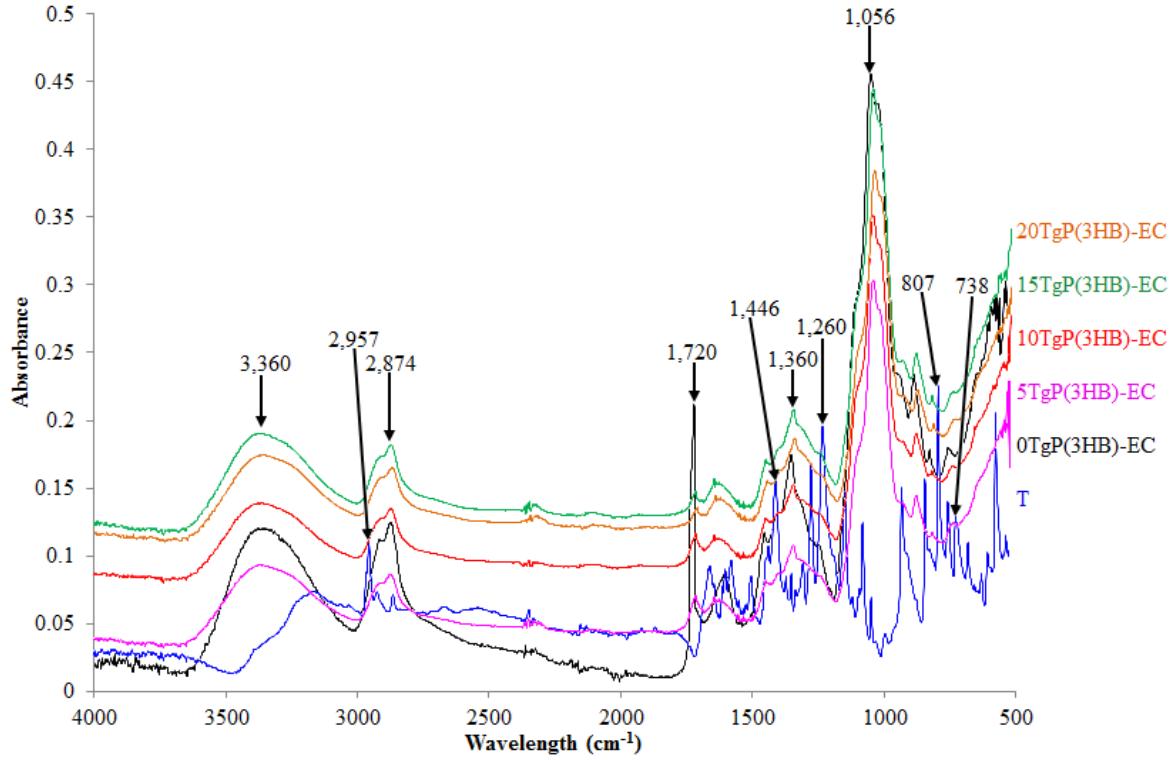
0.5
0.45
0.4
0.35
0.3
0.25
0.2
0.15
0.1
0.05
0
Absorbance
4000
3500
3000
2500
2000
1500
1000
500
Wavelength (cm-1)
3,360
2,957
2,874
1,720
1,446
1,360
1,260
1,056
807
738
20TgP(3HB)-EC
15TgP(3HB)-EC
10TgP(3HB)-EC
5TgP(3HB)-EC
0TgP(3HB)-EC
T

Figure 3

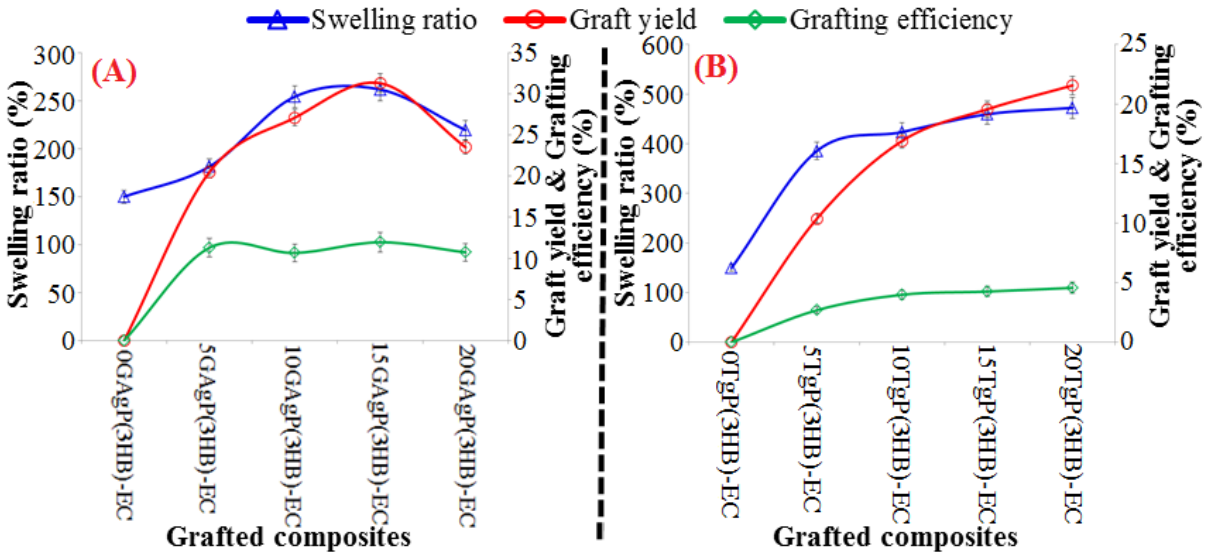
Swelling ratio
Graft yield
Grafting efficiency
(A)
Swelling ratio (%)
Graft yield & Grafting efficiency (%)
0GAgP(3HB)-EC
5GAgP(3HB)-EC
10GAgP(3HB)-EC
15GAgP(3HB)-EC
20GAgP(3HB)-EC
Grafted composites
(B)
Swelling ratio (%)
Graft yield & Grafting efficiency (%)
0TgP(3HB)-EC
5TgP(3HB)-EC
10TgP(3HB)-EC
15TgP(3HB)-EC
20TgP(3HB)-EC
Grafted composites

Figure 4

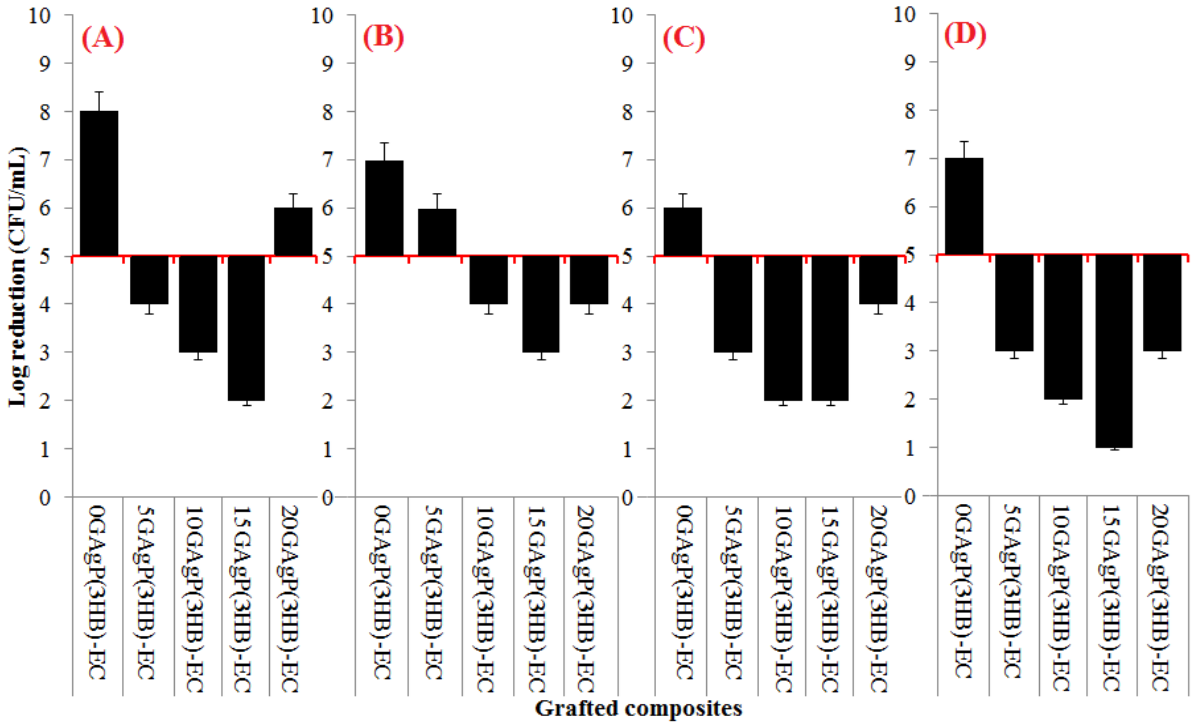
(A)
(B)
(C)
(D)
Log reduction (CFU/mL)
0
1
2
3
4
5
6
7
8
9
10
0GAgP(3HB)-EC
5GAgP(3HB)-EC
10GAgP(3HB)-EC
15GAgP(3HB)-EC
20GAgP(3HB)-EC
Grafted composites

Figure 5

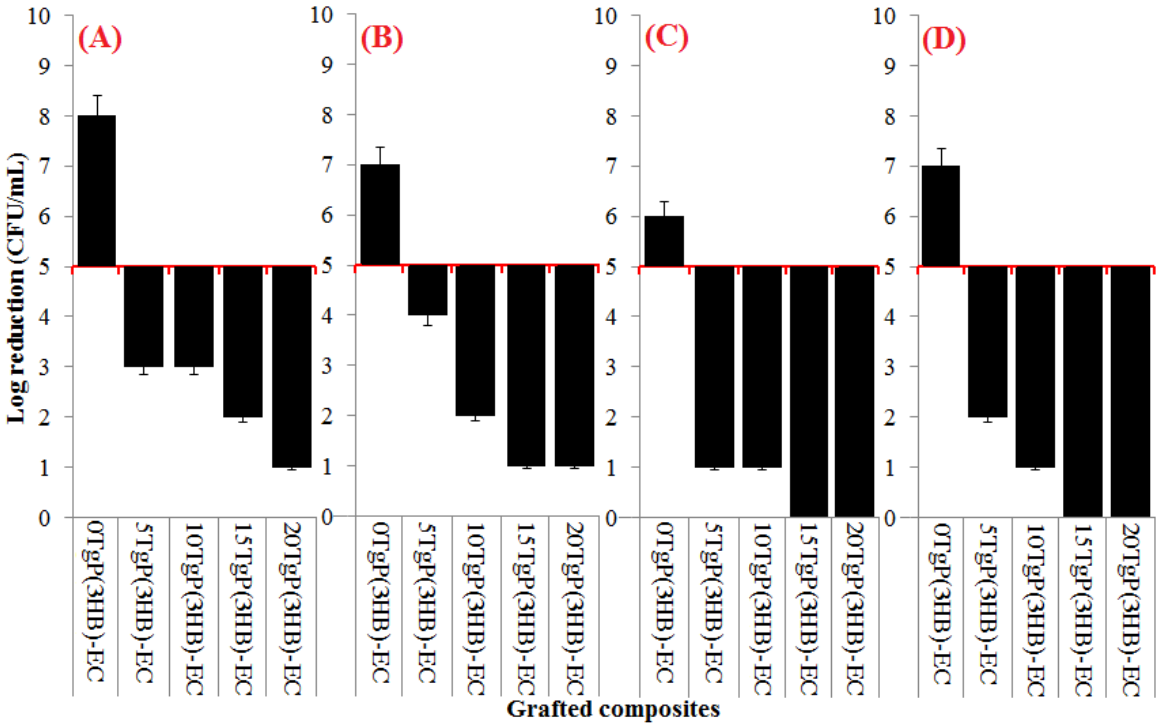
(A)
(B)
(C)
(D)
Log reduction (CFU/mL)
0
1
2
3
4
5
6
7
8
9
10
0TgP(3HB)-EC
5TgP(3HB)-EC
10TgP(3HB)-EC
15TgP(3HB)-EC
20TgP(3HB)-EC
Grafted composites

Figure 6

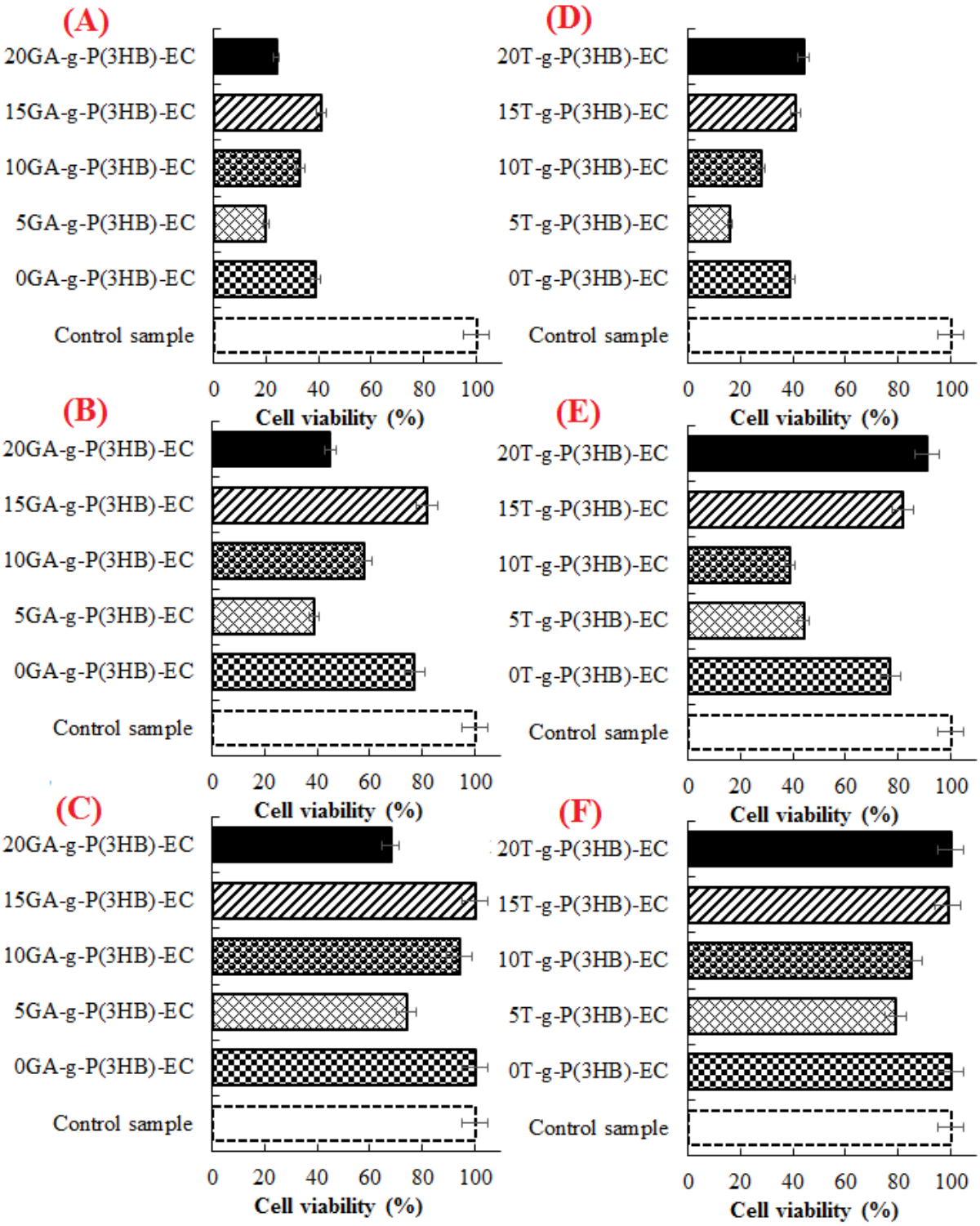
(A)
20GA-g-P(3HB)-EC
15GA-g-P(3HB)-EC
10GA-g-P(3HB)-EC
5GA-g-P(3HB)-EC
0GA-g-P(3HB)-EC
Control sample
0 20 40 60 80 100
Cell viability (%)
(D)
20T-g-P(3HB)-EC
15T-g-P(3HB)-EC
10T-g-P(3HB)-EC
5T-g-P(3HB)-EC
0T-g-P(3HB)-EC
Control sample
0 20 40 60 80 100
Cell viability (%)
(B)
20GA-g-P(3HB)-EC
15GA-g-P(3HB)-EC
10GA-g-P(3HB)-EC
5GA-g-P(3HB)-EC
0GA-g-P(3HB)-EC
Control sample
0 20 40 60 80 100
Cell viability (%)
(E)
20T-g-P(3HB)-EC
15T-g-P(3HB)-EC
10T-g-P(3HB)-EC
5T-g-P(3HB)-EC
0T-g-P(3HB)-EC
Control sample
0 20 40 60 80 100
Cell viability (%)
(C)
20GA-g-P(3HB)-EC
15GA-g-P(3HB)-EC
10GA-g-P(3HB)-EC
5GA-g-P(3HB)-EC
0GA-g-P(3HB)-EC
Control sample
0 20 40 60 80 100
Cell viability (%)
(F)
20T-g-P(3HB)-EC
15T-g-P(3HB)-EC
10T-g-P(3HB)-EC
5T-g-P(3HB)-EC
0T-g-P(3HB)-EC
Control sample
0 20 40 60 80 100
Cell viability (%)

Figure 7

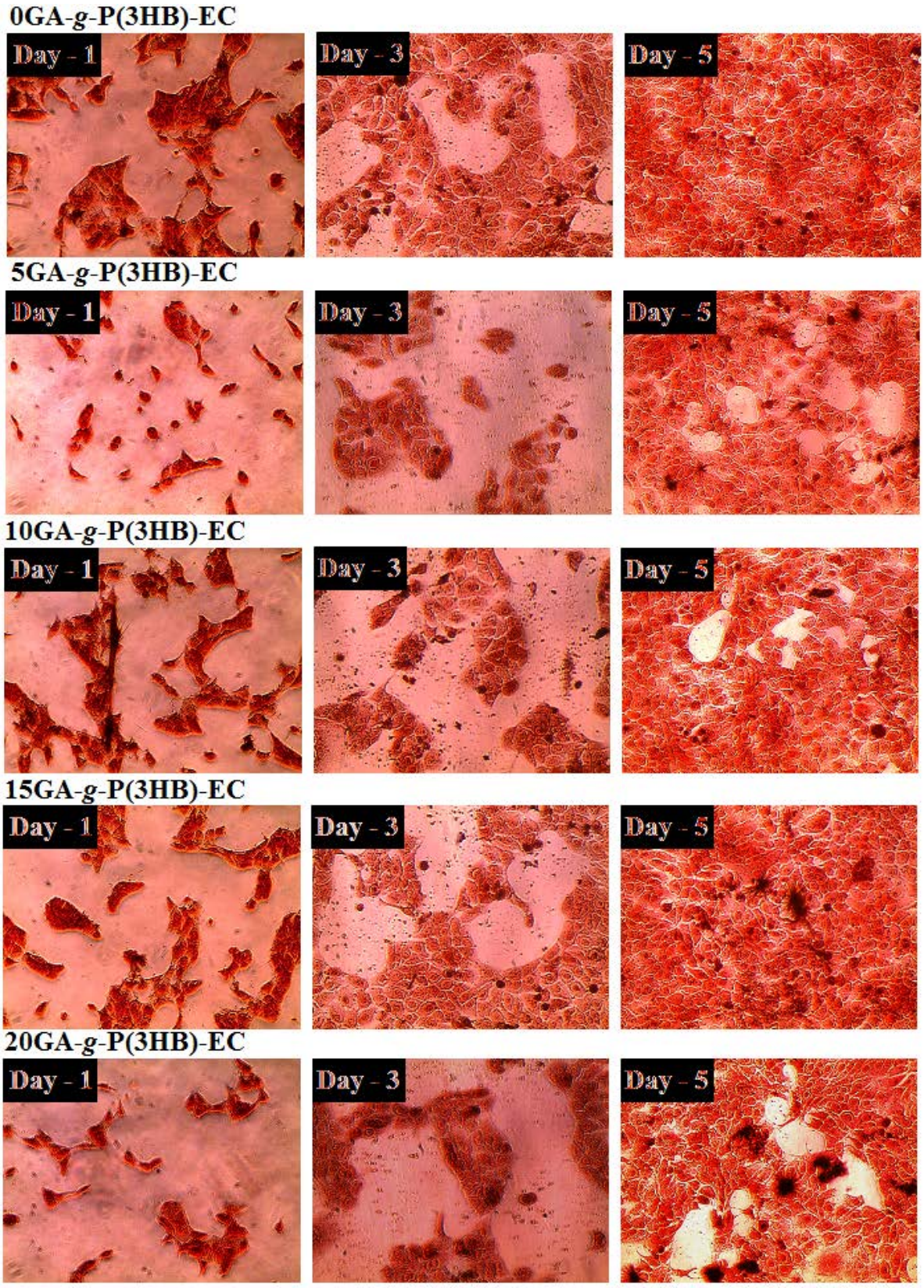
0GA-g-P(3HB)-EC
Day - 1
Day - 3
Day - 5
5GA-g-P(3HB)-EC
Day - 1
Day - 3
Day - 5
10GA-g-P(3HB)-EC
Day - 1
Day - 3
Day - 5
15GA-g-P(3HB)-EC
Day - 1
Day - 3
Day - 5
20GA-g-P(3HB)-EC
Day - 1
Day - 3
Day - 5

Figure 8

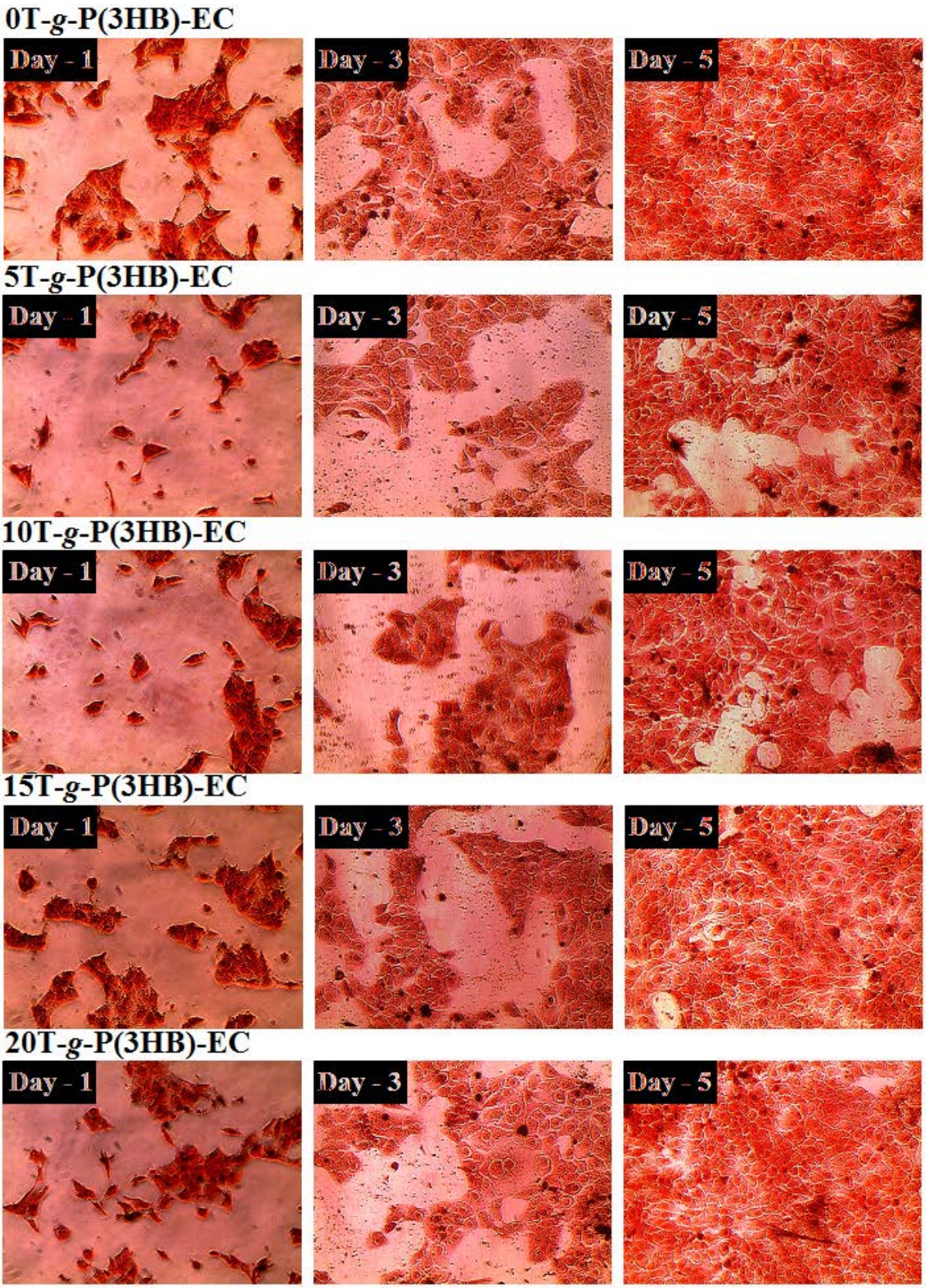
0T-g-P(3HB)-EC
Day - 1
Day - 3
Day - 5
5T-g-P(3HB)-EC
Day - 1
Day - 3
Day - 5
10T-g-P(3HB)-EC
Day - 1
Day - 3
Day - 5
15T-g-P(3HB)-EC
Day - 1
Day - 3
Day - 5
20T-g-P(3HB)-EC
Day - 1
Day - 3
Day - 5

Figure 9

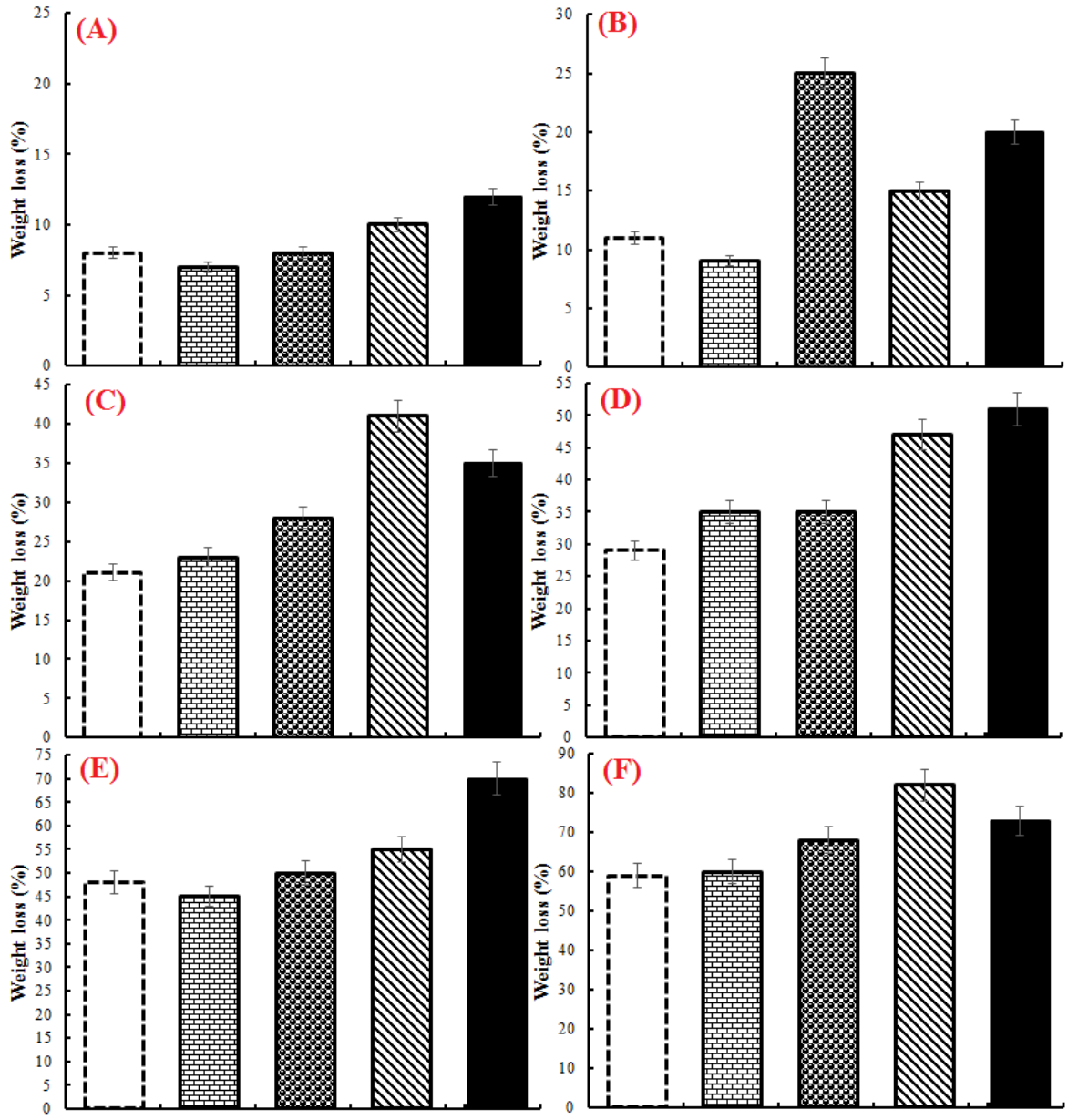

Figure 10

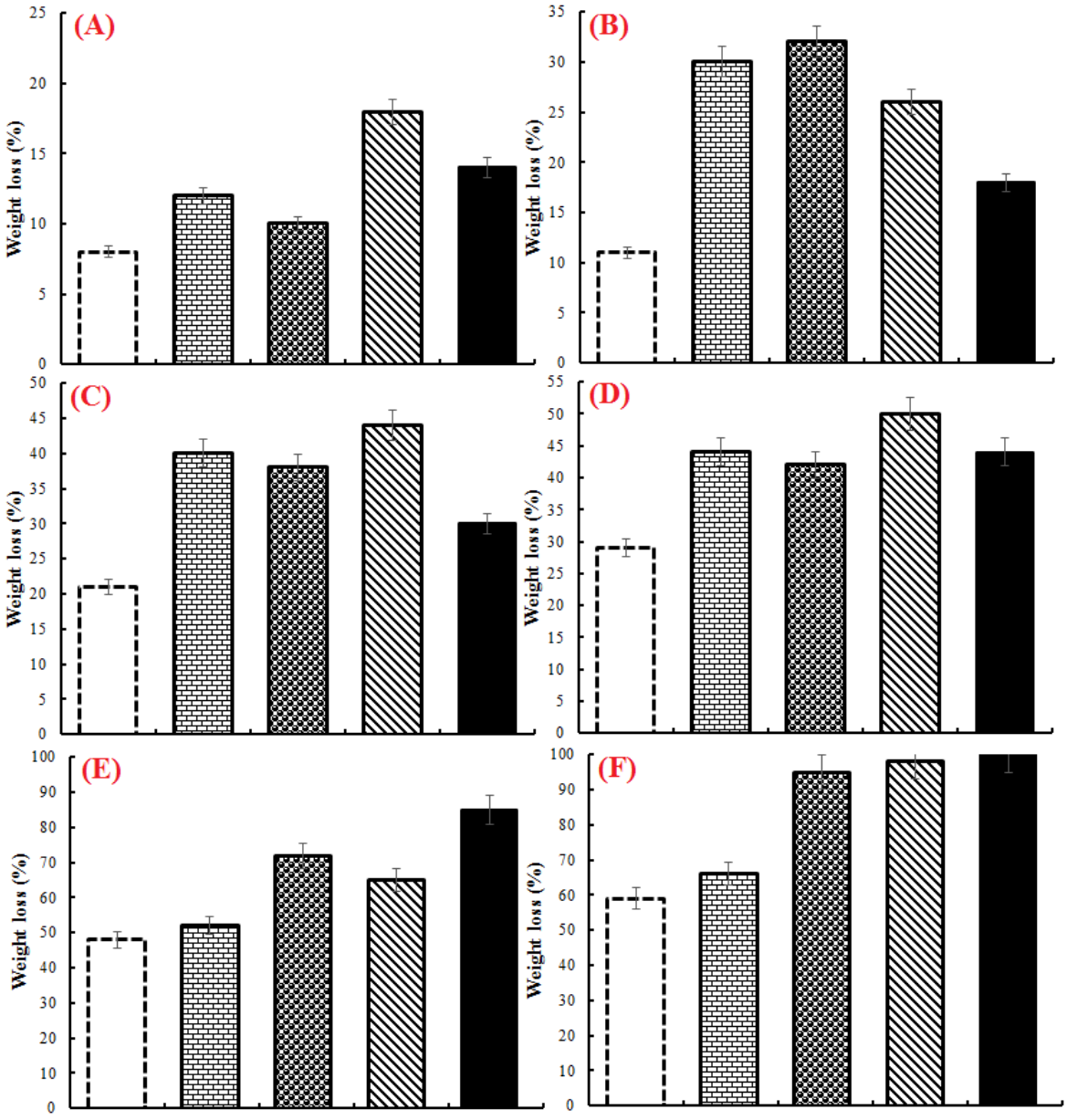

Table 1 Physiochemical characteristics of the natural phenols used in this study for grafting purposes.

Natural phenols	Appearance	Molecular formula	Molecular mass (g/mol)	Density (g/cm^3)	Melting point (^oC)	Functional groups	Structure
Gallic acid	White or yellow-white powder	$C_6H_2(OH)_3COOH$	170.12	1.694	260	Hydroxyl and carboxylic	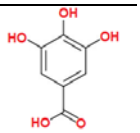
Thymol	White crystalline	$C_{10}H_{14}O$	150.22	0.96	49-51	Hydroxyl